ACS APPLIED MATERIALS & INTERFACES

Research Article

www.acsami.org

Photocurrent Generation in Carbon Nitride and Carbon Nitride/Conjugated Polymer Composites

Joshua C. Byers,[†] Florence Billon,[‡,§] Catherine Debiemme-Chouvy,[‡,§] Claude Deslouis,[‡,§] Alain Pailleret,*[,‡,§] and Oleg A. Semenikhin*[,†]

[†]Department of Chemistry, The University of Western Ontario, London, Ontario, N6A 5B7, Canada.

[‡]CNRS, UPR 15, Laboratoire Interfaces et Systèmes Electrochimiques (LISE, case courrier 133), 4 Place Jussieu, F-75005, Paris, France.

[§]UPMC Université Paris VI, UPR 15, Laboratoire Interfaces et Systèmes Electrochimiques, (LISE, case courrier 133), 4 Place Jussieu, F-75005, Paris, France.

S *Supporting Information*

ABSTRACT: The semiconductor and photovoltaic properties of carbon nitride (CNx) thin films prepared using a reactive magnetron cathodic sputtering technique were investigated both individually and as composites with an organic conjugated polymer, poly(2,2′-bithiophene) (PBT). The CNx films showed an increasing thickness as the deposition power and/or nitrogen content in the gas mixture increase. At low nitrogen content and low deposition power (25−50 W), the film structure was dominated by the abundance of the graphitic sp^2 regions, whereas at higher nitrogen contents and magnetron power CNx films started to demonstrate semiconductor properties, as evidenced by the occurrence of photoconductivity and the development of a space charge region. However, CNx films alone did not show any reproducible photovoltaic properties. The situation changed, however, when CNx was deposited onto conjugated PBT substrates. In this configuration, CNx was found to function as an acceptor material improving the photocurrent generation both in solution and in solid state photovoltaic devices, with the external quantum efficiencies reaching 1% at high nitrogen contents. The occurrence of the donor−acceptor charge transfer was further evidenced by suppression of the n-doping of the PBT polymer by CNx. Nanoscale atomic force microscopy (AFM) and current-sensing AFM data suggested that CNx may form a bulk heterojunction with PBT.

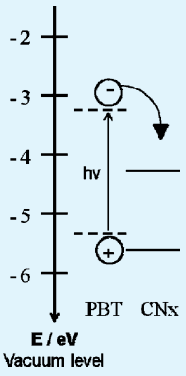

KEYWORDS: *solar cells, bulk-heterojunction, p−n junction, nitrogen doped carbon, photovoltaics, atomic force microscopy*

1. INTRODUCTION

The motivating factors in the development of next-generation photovoltaics are new materials and methods for the fabrication of solar devices on a large scale and at a low cost. Polymer solar cells represent a promising opportunity toward the realization of this goal for several reasons, such as high absorption coefficients that permit the use of extremely thin films, which significantly reduces the materials costs, as well as the ability to use high throughput fabrication techniques such as jet printing, spray-coating, etc.[1,2] The vast majority of polymer solar cells studied at present use fullerenes and their derivatives as the ubiquitous acceptor materials which enhance exciton dissociation in conjugated polymers upon light absorption.[3−5] The overwhelming use of fullerenes is due to their exceptional electron-accepting abilities combined with efficient electron transport properties.[6,7] The resulting active layer of a polymer solar cell typically contains 50% or more of a fullerene acceptor mixed together with a donor p-type conjugated polymer in a complex fashion forming a so-called bulk heterojunction, with exciton dissociation and photoinduced charge transfer occurring on the nanoscale between the interdispersed and very finely phase segregated donor and acceptor phases.[8] Another very important role of the fullerene phase is to provide conducting pathways throughout the photoactive film to ensure efficient extraction of photogenerated carriers.

Overall, to ensure high efficiency, a polymer donor−acceptor solar cell should have a very specific and very fine nanostructure, which should also be maintained throughout the cell service life.[9] The difficulty in creating and maintaining such an intricate nanostructure between the donor and acceptor phases remains one of the limiting factors on the way to commercially viable polymer donor−acceptor solar cells.[10−13] The other issues with fullerenes as acceptors are their low-lying LUMO that limits the cell output voltage, as well as the need to use high fullerene loading ratios, which increases costs and reduces the absorption of light by the active layer (the majority of solar light in polymer photovoltaic devices is absorbed by the polymer and not by the fullerene).[5] Therefore, there is a need to search for alternative acceptor materials for polymer donor−acceptor cells.[14,15] The new acceptor materials should not only possess superior electron-acceptor properties and suitable LUMO position but must also ensure efficient

Received: May 27, 2012
Accepted: August 10, 2012
Published: August 10, 2012

   dx.doi.org/10.1021/am3009482 | *ACS Appl. Mater. Interfaces* 2012, 4, 4579−4587

transport of photogenerated carriers[16] (which has been a major stumbling block for many molecular donor−acceptor systems) while remaining economically viable.

Semiconducting carbon films and their composites have attracted the attention of researchers for their potential use in optical and electronic devices.[17,18] Vacuum-sputtered carbon nitrides (CNx) are a potential new class of semiconductor materials that have not yet received sufficient attention for photovoltaic applications.[19−22] The majority of research to date has focused on the outstanding mechanical and electrochemical properties of CNx,[23−26] whereas carbon nitrides appear to be a very promising material for potential photovoltaic device applications due to their n-type semiconductor properties,[27] high absorption coefficient in the visible region,[28] tunable electronic and optical properties,[22] chemical robustness and inertness,[29] etc.

However, to the best of our knowledge, there has only been one report of a photovoltaic effect observed in a vacuum deposited highly sp^2 hybridized CNx material, with the photocurrent produced being very low.[20] This may be a result of the high defect density present in these materials due to their amorphous nature.[30] We ourselves have not succeeded in obtaining appreciable and reproducible photocurrents from vacuum deposited CNx films (see below). However, we were able to show, for the first time, that vacuum-deposited CNx can serve as an efficient electron acceptor in organic conjugated polymer-based solar cells. This was also confirmed by electrochemical and photoelectrochemical measurements. Taken together with our data on the nanoscale structure of CNx films deposited onto conjugated polymer substrates,[31] it is likely that CNx is able to form a bulk heterojunction with the donor conjugated polymer phase. These results suggest that CNx may be an interesting practical alternative to fullerenes as they have the potential to overcome some of the drawbacks associated with such acceptor materials. Moreover, unlike the randomly dispersed films obtained with solution deposited polymer−fullerene mixtures, the interpenetrating network formed by vacuum-deposited CNx throughout the polymer matrix should be quite stable. This may be beneficial for the improvement of the lifetime of the bulk heterojunction structure for polymer-based solar cells.

The influence of the deposition parameters such as deposition power and nitrogen content on the structure and electronic and optical properties of highly sp^2-hybridized CNx materials was also studied. It is well-known that the deposition parameters for vacuum-deposited carbon nitride films have a significant impact on their structure and therefore on their optical and electronic properties.[32−37] The incorporation of nitrogen into amorphous carbon promotes the clustering of carbon nitride sp^2 domains, with a variety of possible bonding configurations, while decreasing the long-range order of the graphitic domains.[36,38] The decrease in the graphitic domains and increase in the amount of CNx nanoclusters should lead to improved semiconductor properties and thus improved photoefficiency.[21]

2. EXPERIMENTAL SECTION

Substrates. Indium tin oxide (ITO)-coated glass electrodes (R_s = 4−8 Ω) were purchased from Delta Technologies, Ltd. The electrodes were sonicated successively in detergent, water, acetone, ethanol and deionized water and dried in an oven at 90 °C after removing residual water with nitrogen gas. 3,4-Ethylenedioxythiophene (EDOT) (Aldrich, 97%) was used as received. 2,2′-Bithiophene (BT) (Aldrich, 97%) was purified by vacuum sublimation. Galvanostatic electrochemical deposition was used to deposit thin films of poly(3,4-ethylenedioxythiophene) (PEDOT) and poly(2,2′-bithiophene) (PBT). PEDOT was prepared from a solution containing 0.37 M EDOT and 0.1 M tetrabutylammonium hexafluorophosphate ($TBAPF_6$) in acetonitrile. PBT was prepared from a solution containing 5×10^{-3} M 2,2′-bithiophene and 0.1 M $TBAPF_6$ in acetonitrile. Films were rinsed in pure acetonitrile following deposition to remove excess monomer and electrolyte from the electrode surface.

Vacuum Deposition of Carbon Nitride. Deposition of carbon nitride films was performed using direct current (DC) reactive cathodic magnetron sputtering in a custom built vacuum deposition system or in a commercial reactor (MP 300 S model, Plassys, France). For each CNx deposition, the total pressure in the vacuum chamber was 1 or 10 Pa using a mixture of pure Ar gas with pure N_2 gas. The N_2 partial pressure was varied from 5 to 50% of the total deposition pressure to prepare films with different nitrogen contents. The deposition power was varied at 25, 50, and 100 W. The deposition time was 20 min. The nitrogen content in the films increased with an increase in the nitrogen content in plasma and was determined from the atomic ratio of nitrogen and carbon obtained from the XPS spectra (see the Supporting Information).

Film Characterization. The film thicknesses for the deposition conditions employed in this work were determined from the observation of cross-sections of the samples using scanning electron microscopy (FEG-SEM, Ultra55, Zeiss) images and are presented in the Supporting Information. A U4001 spectrophotometer (Hitachi) was used to acquire the UV−vis−IR spectra of CNx films. All spectra were baseline corrected to take into account absorption by the indium tin oxide coated glass slides. XPS analyses were carried out at ITODYS laboratory (Paris, France) using a VG ESCALAB 250-iXL spectrometer. The X-ray source was monochromatic Al Kα radiation (1486.6 eV). The survey spectra were recorded with a pass energy of 100 eV, whereas the high-resolution spectra were recorded with a pass energy of 20 eV in the constant analyzer energy mode. The spot size was ca. 500 μm. The photoelectron takeoff angle was of 90° with respect to the CN_x surface. Each spectrum was background corrected using the Shirley's method. All the binding energy (BE) scales were referenced by setting the C1s main contribution BE to 285 eV.

Device Architecture. Three separate types of device architectures were prepared for measurement in either solution or a solid state configuration. For solution measurements, the substrates consisted of CNx vacuum deposited onto ITO electrodes (ITO/CNx) or CNx films deposited onto PBT coated ITO substrates (ITO/PBT/CNx). Solid-state CNx based devices were prepared in either a sandwich ITO/CNx/Au configuration or using a standard photovoltaic architecture of ITO/PEDOT/PBT/CNx/Al with PBT being a donor conjugated polymer and CNx being an acceptor. Au and Al contacts were fabricated by thermal evaporation.

Device Characterization. Electrochemical and solid state solar cell measurements were performed using a PAR 263A potentiostat−galvanostat (Princeton Applied Research) coupled with a Solartron 1250 frequency response analyzer. Steady state measurements were controlled using version 3.1 CorrWare software and frequency domain measurements were controlled using version 2.8 ZPlot software (Scribner Associates Inc.). The light source used was a 405 nm, 20 mW laser diode (LD1510, Power Technology) having a light intensity of 2×10^{17} photons s^{-1} cm^{-2} (90 mW cm^{-2}). Pyrex glass cells without separation of the anodic and cathodic compartments were used for all electrochemical and photoelectrochemical measurements. The cells were purged with Ar gas and sealed prior to measurement. Silver wire quasi-reference electrodes were used for all measurements. To ensure their reproducibility, the reference electrodes were prepared and stored in solutions of the corresponding measurement electrolyte.[39−42] Cyclic voltammetry measurements were performed in acetonitrile (<35 ppm H_2O) using 0.1 M $TBAPF_6$ (Fluka, > 99%) as the supporting electrolyte. A scan rate of 100 mV s^{-1} was used for all measurements. Mott−Schottky and photoelectrochemical measurements were carried out in aqueous solutions made with Millipore deionized water with 0.1 M KCl as the supporting electrolyte. The

Mott–Schottky measurements were performed using an ac amplitude of 10 mV rms at a frequency of 6.626 kHz, which was verified to be high enough for the electrode impedance to be well-approximated by a serial RC circuit.

Atomic Force Microscopy. Current sensing AFM (CS-AFM) measurements were carried out to characterize the local nanoscale conductivity and distribution of conducting domains in the carbon nitride/conjugated polymer composites. These measurements were performed in air simultaneously with the acquisition of the topography data generating spatially resolved images of the local conductivity and morphology of the samples. A multimode AFM (Veeco Metrology) equipped with a Nanoscope IV controller (Veeco) and a CS-AFM extension module was used. The measurements were performed in contact mode using DDESP conducting diamond coated AFM probes (Nanoworld, typical force constant 0.35 N/m). A bias of +500 mV was applied to the AFM tip with respect to the sample and therefore the conducting regions (regions of higher positive currents) appear bright in these images (the positive current direction is from the sample into the tip).

3. RESULTS AND DISCUSSION

Characterization of Vacuum-Deposited CNx Films. *Conductivity of CNx.* The electronic properties of carbon nitride are highly dependent upon the local bonding and structure formed throughout the CNx film. Because of the large number of techniques available to create these materials, it is useful to classify CNx as highly sp^2 hybridized carbon nitride, which is quite different from the highly sp^3-hybridized nitrogen doped diamond.[33] The enhanced conductivity of highly sp^3 hybridized nitrogen doped diamond has been attributed to sp^2-rich CNx grain boundaries.[43] Therefore, it is of interest to prepare CNx materials that are predominantly sp^2-hybridized as it is the π and π^* states that control the electronic and optical properties of these materials.[44] There are still many aspects of the deposition process and its impact on the film properties that are not well understood due to the large number of deposition parameters. The target power and nitrogen content in the gas plasma have both been shown to modify the local structure as well as the amount of nitrogen that is incorporated into CNx films.[45] The amount of nitrogen incorporated into highly sp^2 hybridized DC and RF sputtered CNx is known to modify the local bonding and structure, which directly affects the electronic properties.[22,36]

Figure 1 shows the conductivity as a function of nitrogen content for CNx films prepared at different magnetron powers. For these measurements, we used a solid state architecture that consisted of a CNx layer sandwiched between ITO and Au electrodes taking into account the variations in the film thicknesses with the deposition conditions (see the Supporting Information). The conductivity of CNx did not vary significantly for target powers of 25 and 50 W. It has been shown previously that carbon nitride films prepared at low deposition powers have a significant graphitic structure.[46] The higher conductivity observed in films prepared at lower target powers is a result of the graphitic structure which contains a significant density of energy levels in the midgap region, which facilitate electronic conduction. Such graphitic regions may be localized at grain boundaries as discussed in the literature[43] and form percolation conduction paths inside the films bypassing semiconducting nitrogen-rich domains. This can explain the virtual independence of the films conductivity at low powers on the nitrogen content.

For films prepared at 100 W, the conductivity decreases almost 3 orders of magnitude with increasing nitrogen content. The dramatic decrease in conductivity cannot be attributed to

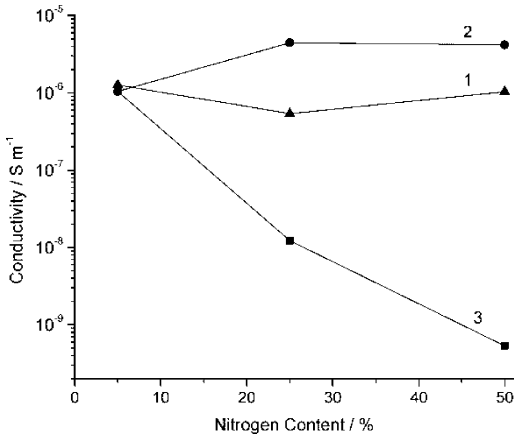

Figure 1. Conductivity of CNx films as a function of N_2 content in the gas mixture for films prepared with a deposition power of 25 W (plot 1), 50 W (plot 2), 100 W (plot 3) during deposition. The deposition time for all films was 20 min. The lines are guides for the eye.

thickness variations as the conductivity values presented were corrected for the differences in film thickness. The significant drop in conductivity at increased target power and nitrogen content can be attributed to structural and chemical modifications of the films. This suggests that films prepared at higher target powers and nitrogen concentrations contain less graphitic sp^2-hybridized material and therefore less percolation pathways that likely determine the conductivity in materials obtained at lower powers. This hypothesis is further supported by the changes in conductivity for a CNx film under illumination reported below.

Photoconductivity of CNx. For all CNx films, the conductivity was examined in the dark and under illumination. There have been previous reports of photoconductivity in tetrahedral CNx and for highly sp^2-hybridized CNx.[47,48] In this work it was found that CNx films prepared at low powers showed little or no change in conductivity under illumination for the deposition parameters examined. The curves (not shown) showed Ohmic behavior. It was only films prepared at 100 W and nitrogen contents of 25% and 50% that showed a significant change in their conductivity under illumination, or photoconductivity. Figure 2 shows typical $J-V$ plots measured in the dark and under illumination for an ITO/CNx/Au sandwich device prepared at 100 W and 50% N_2. It is seen that

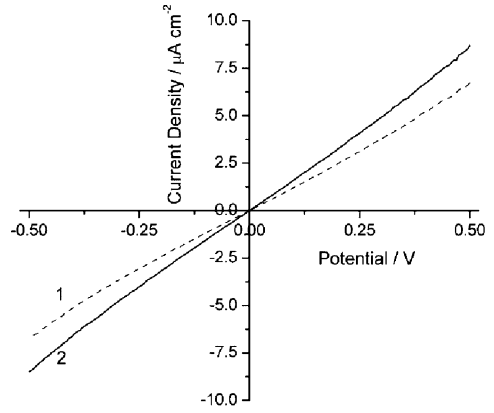

Figure 2. Dark conductivity (plot 1) and photoconductivity (plot 2) for ITO/CNx/Au. CNx was prepared at 100 W and 50% N_2.

the slope of the $J-V$ plots increases under illumination indicating an increase in the film conductivity. However, the linear character of the J-V plots indicates that even at high powers and nitrogen contents the films retain their Ohmic behavior and show no rectification that could be expected for an n-type semiconductor in a Schottky diode configuration. Also, no photovoltage has been detected. Taken together with the lack of photoconductivity in the films prepared at lower target powers, these facts suggest that for all investigated films the conductivity through graphitic percolation pathways still remains the dominant conductivity mechanism. For films prepared at lower powers, the graphitic content is too high for any significant increase in the carrier concentration under illumination. At the same time, the occurrence of photoconductivity at higher powers and nitrogen contents suggests that indeed there is photogeneration of carriers in nitrogen-enriched domains, which therefore do exhibit semiconductor behavior. However, due to the presence of a percolating graphitic phase, these carriers cannot give rise to a photovoltaic effect and produce photoconductivity instead. This hypothesis correlates well with the results of photovoltaic measurements of CNx films deposited onto conjugated polymer substrates presented below and explains why there were no reproducible observations of the photovoltaic effect in CNx films. It can be anticipated that such an effect could still be found if one eliminates the percolation conductivity pathways due to increased sp^2 graphitic content, perhaps, by means of a post-treatment of CNx materials.

Evidence of Space Charge Formation in CNx Films. The above hypothesis is supported by the fact that, despite showing no photovoltaic properties, CNx films were still found to sustain the formation of a space-charge layer consistent with their being n-type semiconductors. This was confirmed by Mott−Schottky measurements. The Mott−Schottky measurements analyze the evolution of the capacitance of a semiconductor electrode with the applied bias. If a space-charge region is formed inside the semiconductor electrode, this capacitance should follow the Mott−Schottky law,[39] which is given by the following equation

$$\frac{1}{C_{SC}^2} = \left(\frac{2}{e_0 N_D \varepsilon \varepsilon_0 A^2}\right)\left(E - E_{fb} - \frac{kT}{e_0}\right) \quad (1)$$

where C_{SC} is the space charge capacitance, ε is the dielectric constant of the semiconductor, ε_0 is the permittivity of free space, e_0 is the elementary charge, A is the electrode surface area, $E - E_{fb}$ is the potential drop across the space charge region in the semiconductor, k is the Boltzmann constant, and T is the absolute temperature.

It follows from the Mott−Schottky law that, if a space-charge layer is formed in the semiconductor, the experimental dependence of the inversed squared capacitance on the applied bias should have a linear portion (the deviations from linearity are usually related to the finite thickness of the semiconductor layer or potential redistribution at the contacts).[39,42] In this case, the slopes of the linear portions of the Mott−Schottky plots allow one to find the density of the space charge within the space charge region, or the dopant density. The intercepts of the Mott−Schottky plots on the X-axis produce the value of a so-called flat-band potential, which is related to the work function of the semiconductor material. It is important to emphasize that Mott−Schottky measurements are performed using ac modulation of the applied voltage and thus, unlike steady-state measurements, are able to distinguish between the resistive effects because of heterogeneity of the semiconductor material and the presence of percolation conductivity pathways, and the capacitive behavior originating from the formation of the space-charge region.

The Mott−Schottky measurements were performed in solution with a so-called electrolytic contact.[39,49] The use of a solution contact is often advantageous for the characterization of semiconductor materials since such an arrangement allows one to avoid complications arising at solid cell contacts (poor energy level matching, high recombination rate, chemical compatibility, etc.).

Figure 3A shows a typical Mott−Schottky plot for a CNx film in an aqueous solution. Similar plots were obtained for the other CNx films except for CNx films prepared at 100 W and 50% N_2, which could not be characterized due to the well-known delamination in solution of CNx films prepared at higher deposition powers and nitrogen contents.[50] All Mott−Schottky plots showed distinct linear portions that had a positive slope with increasing positive potential. This behavior is typical for n-type semiconductor materials and clearly indicates the formation of a space-charge region.[51]

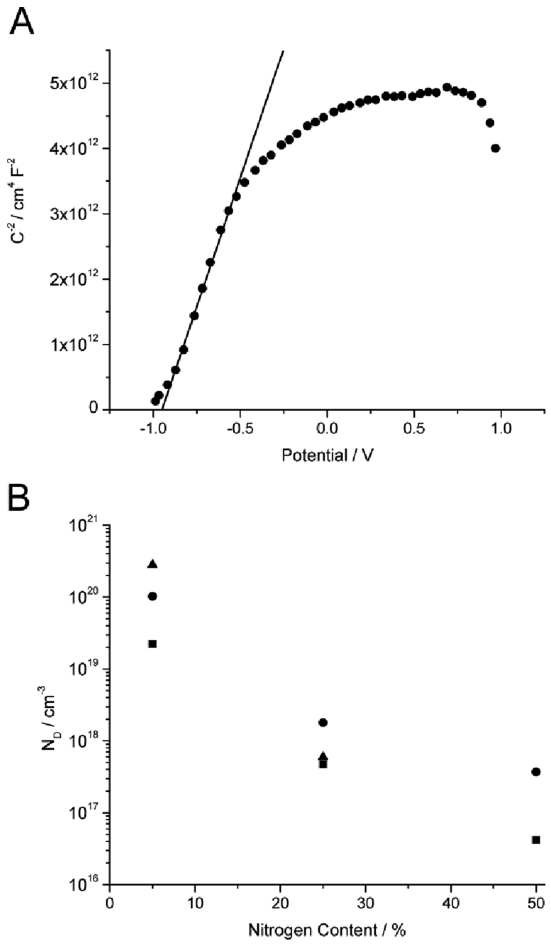

Figure 3. (A) Mott−Schottky plot for CNx on an ITO substrate in aqueous 0.1 M KCl. CNx was prepared at 50 W and 25% N_2. (B) Donor density determined from slopes of Mott−Schottky plots for CNx films as a function of nitrogen content for deposition powers of 25 W (■), 50 W (●), and 100 W (▲).

Figure 3B shows the dependence of the donor density of CNx extracted from the linear portions of the Mott−Schottky

plots on the nitrogen content for target powers of 25, 50, and 100 W. The deposition power was not found to have a significant effect on the donor density, whereas a clear decrease in the donor density was observed for increasing nitrogen contents. This is a very interesting result as it is nitrogen that functions as an n-type dopant in the carbon film to produce an n-type semiconductor. Therefore, one could expect that the dopant density would increase, not decrease with an increase in the nitrogen content.

A possible explanation may be related to the well-known fact that nitrogen is able to act as a dopant only in certain bonding configurations.[52] In addition, the dopant density may be affected by disorder in a semiconductor material that increases the density of charge trapped in the space-charge layer. It is known that an increase in the nitrogen content in the films is accompanied by an increase in the number of nitrile groups.[53] The nitrile groups are bond terminating and thus, with increasing nitrogen content, there should be a decrease in the size of the carbon nitride clusters, which could also be accompanied by a decrease in the degree of disorder. Such changes may or may not be accompanied by an increase in the total nitrogen content in the film. It has been shown that the amount of nitrogen incorporated into CNx films increases as the nitrogen content used during deposition increases and then plateaus beyond approximately 30−40% N_2 in the gas plasma.[54] For films prepared at 25 and 50 W, nitrogen contents in the plasma chamber of 5−50% led to a nitrogen content in the film of ca. 20−45%, as determined using XPS (see the Supporting Information). As well, it was found for films prepared at 50 W that the nitrogen sp^2/sp^3 ratio remained practically constant at ca. 0.44/0.56, regardless of the nitrogen content in the films, which indicates that the main effect of adding nitrogen to the plasma during deposition is to increase the total nitrogen content in the films without significantly modifying the relative proportion of sp^2 and sp^3 nitrogen regions.

Therefore, our results suggest that an increase in the nitrogen content in the gas plasma not only decreased the sp^2 graphitic content but also increased the total amount of nitrogen contained in the film. Furthermore, the Mott−Schottky experiments demonstrate that the amount of nitrogen used during deposition has a greater affect on the dopant density than does the target power, while the conductivity measurements indicate that the deposition power has a significant impact on the electronic structure of the film. These results once again demonstrate the complexity of the CNx deposition mechanism and the need for a more detailed understanding of the influence of the deposition conditions on the electronic and semiconductor properties of CNx films. However, it was demonstrated that the semiconductor properties of CNx films were the best for films deposited at high power and high nitrogen contents, which featured the lowest parasitic conductivity and the most developed space charge region.

Photocurrent Generation in CNx/Polymer Composites. As was shown above, CNx films alone did not show any photovoltaic effect but still demonstrated the ability of charge carrier photogeneration, as evidenced by the conductivity changes under illumination, and the formation of a space charge layer, as evidenced by Mott−Schottky measurements in solution. These effects were consistent with the anticipated n-type semiconductor behavior. It was therefore of interest to combine n-type CNx materials with a p-type conjugated polymer. In our earlier paper, we demonstrated the possibility of the preparation of such composite materials by vacuum deposition of CNx films onto the conjugated polymer poly(2,2′-bithiophene) (PBT).[31] In this work, we test similar CNx/polymer composites for photocurrent generation in both solid-state configuration and in solution.

Figure 4 shows an energy level diagram expected for a CNx and polybithiophene interface based on the work function,

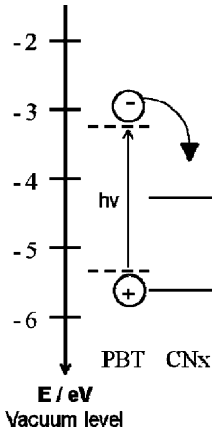

Figure 4. Energy level diagram of a CNx/PBT interface illustrating the proposed photoinduced electron transfer from PBT to CNx.

electrochemical and optical data for CNx and PBT. The work function of CNx was shown in the literature to be ca. 5.1 eV and did not depend on nitrogen or sp^2/sp^3 carbon content.[55,56] The optical gap can vary to some extent with nitrogen and sp^2 content (see the Supporting Information), the average value of the bandgap was 1.3 eV. Therefore, the VB and CB edges for CNx were estimated to be −5.75 and −4.45 eV, respectively. The HOMO/LUMO levels of PBT have been determined from the onset of electrochemical oxidation and reduction respectively (see Figure 9 below) to be −5.45 and −3.35 eV. Therefore, the conduction band edge of CNx lies ca. 1.1 eV lower in energy than the PBT LUMO level, which should make CNx an efficient electron acceptor material.

Photocurrent Measurements in Solid State and in Solution. Photoelectrochemical measurements were performed in aqueous conditions using KCl as a supporting electrolyte. Polythiophene-based electrodes have been shown to exhibit cathodic photocurrents during illumination under these conditions.[57] For our measurements, carbon nitride films were deposited onto PBT-coated ITO substrates. It should be noted that CNx films deposited onto ITO substrates without PBT exhibited little or no photocurrent generation in aqueous solution, consistent with the results obtained in solid-state sandwich devices. Therefore, photocurrent generation will occur because of light absorbed in the PBT layer. Figure 5 shows photocurrent measurements for films prepared at 25 W and nitrogen contents of 5, 25, and 50%. The electrodes were illuminated through the CNx layer. It can be seen that the CNx/PBT composite films exhibit a substantially higher photocurrent than the pristine PBT film. Since the measured photocurrent remained cathodic, and in view of the demonstrated inability of CNx films alone to generate a photocurrent, this fact suggests that the enhanced photocurrent generation observed with the CNx/PBT composite films should be attributed to CNx functioning as an acceptor material when incorporated with a donor conjugated polymer such as polybithiophene. The same behavior is also observed for a solid state configuration. Figure 6 shows photocurrent−

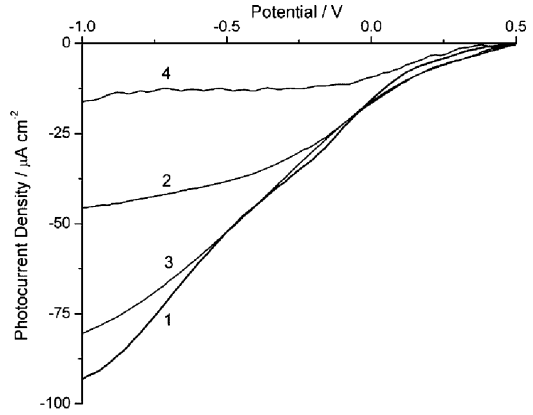

Figure 5. Net photocurrent generation of PBT/CNx composites on ITO substrates in aqueous 0.1 M KCl. CNx films were prepared at 25 W and nitrogen contents of 5% (plot 1), 25% (plot 2), and 50% (plot 3). Photocurrent generation of a pristine PBT film is included for comparison (plot 4).

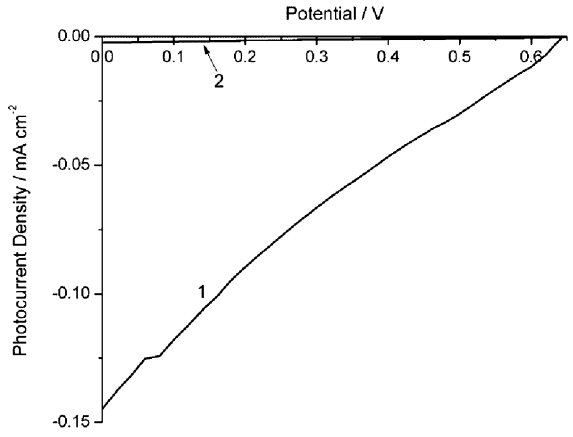

Figure 6. Current−Voltage plot of a solid state ITO/PEDOT/PBT/CNx/Al (plot 1) and a ITO/PEDOT/PBT/Al (plot 2) photovoltaic device. CNx film was prepared at 25 W and 10% N_2.

voltage curves obtained for two solid state organic photovoltaic devices with and without CNx. The results clearly demonstrate the improvement in photocurrent generation when CNx is incorporated into a polymer based solar cell (plot 1) compared to a device without CNx (plot 2).

It is natural to assume that the magnitude of the photocurrent enhancement will correlate with the improvement in the semiconductor properties of CNx films and therefore the greatest enhancement will be observed for films with the highest nitrogen content. The results of Figure 5 do not suggest such an outcome. However, we must remember that variations in the deposition conditions affect the CNx film thickness and therefore, since the illumination for films measured in Figure 5 was performed from the CNx side, the amount of light that was absorbed by the donor PBT phase will be reduced by light absorbed in the CNx layer. The required correction can be performed using the data on CNx film thicknesses and absorption coefficient that are found in the Supporting Information. The results are presented in Figure 7. It is seen that, after the correction, the improvement in the photocurrent clearly correlates with an increase in the nitrogen concentration and therefore in the carbon nitride content in the films. One can see that the external quantum efficiency of the best photoelectrochemical cell at 50% nitrogen content exceeds 1%,

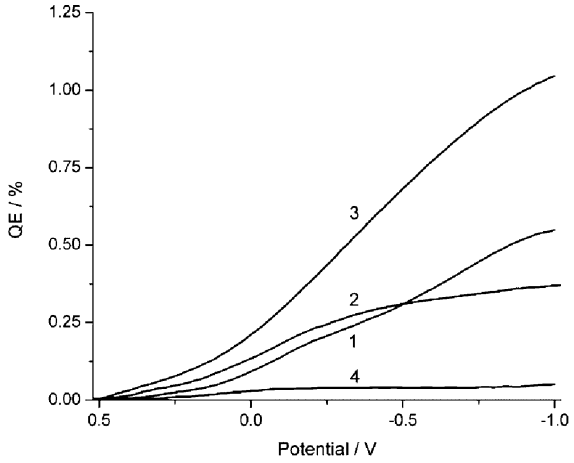

Figure 7. Quantum efficiency of PBT/CNx composites on ITO substrates in aqueous 0.1 M KCl. CNx films were prepared at 25 W and nitrogen contents of 5% (plot 1), 25% (plot 2), and 50% (plot 3). A pristine PBT film is included for comparison (plot 4). Scan rate: 100 mV s^{-1}.

which is a relatively good result taking into consideration that no optimization of the cell structure and composition, especially that of the donor layer, was performed. Future work will focus on tuning the properties and nanostructure of the bulk heterojunction layer, for instance, by thermal annealing, as well as exploring inverse architecture devices with polymer layers deposited onto CNx using high work function metal electrodes. However, the results of this work allow us to conclude that vacuum deposited CNx films may eventually become a viable alternative to PCBM and other fullerene-based acceptors in polymer donor−acceptor photovoltaic cells.

Nanoscale Structure of CNx/Polymer Composites. Furthermore, there is evidence to suggest that the vacuum-deposited CNx films penetrate through the conjugated polymers forming a kind of bulk heterojunction rather than a bilayer structure. The ability to form a bulk heterojunction between the donor and acceptor phases is an important feature for polymer-based solar cells due to the short exciton lifetimes and limited electron and hole mobility.[8] Specifically, it was shown using nanoscale conductivity measurements through a conducting AFM tip that the CNx/conjugated polymer composites exhibit a complex structure coherent with CNx penetrating into the conjugated polymer as a consequence of the deposition technique and forming a nanoscale blend with alternating regions of high and low conductivity and nitrogen content.

The observed structure is illustrated in Figure 8, which presents simultaneous topography (left) and CS-AFM current (right) images of a PBT/CNx composite film. The conductivity image clearly shows finely segregated nanoscale regions of high and low conductivity that can be attributed to conducting and semiconducting CNx domains within the PBT film. Such complex structures were not found for either CNx films deposited onto ITO substrates or PBT films alone.[31] Importantly, the conductivity of the same PBT films without CNx was much lower indicating that CNx indeed penetrated the polymer layer and formed a kind of interpenetrating bulk heterojunction structure. Importantly, CNx did penetrate the PBT films but did not short-circuit them, as evidenced by electrochemical data (see below). At the same time, as was

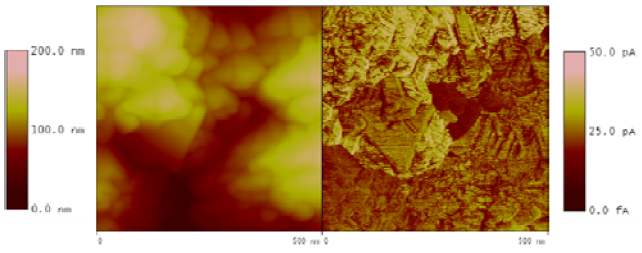

Figure 8. 500 nm by 500 nm topography (left) and CS-AFM current (right) images of a CNx film on PBT. A bias of +500 mV was applied to the tip. Height scale bar: 200 nm. CS-AFM current scale bar: 50 pA.

evidenced by our previous XPS measurements,[31] the outmost layers of CNx/polymer composites contained CNx only without PBT (no sulfur was found on the composite surface), which suggested that we could have a hybrid structure combining bilayer and bulk heterojunction architectures. However, regardless of the type of nanostructure, CNx/polymer composites under study were able to provide an efficient donor–acceptor charge separation as described in the previous sections.

Electrochemical Evidence of the Donor–Acceptor Effect. The occurrence of the donor–acceptor effect in CNx/PBT composites was supported by electrochemical measurements of the anodic and cathodic doping of the PBT polymer with and without CNx. The corresponding cyclic voltammograms for a PBT electrode and PBT/CNx composite electrode in acetonitrile are shown in Figure 9. A cyclic voltammogram of

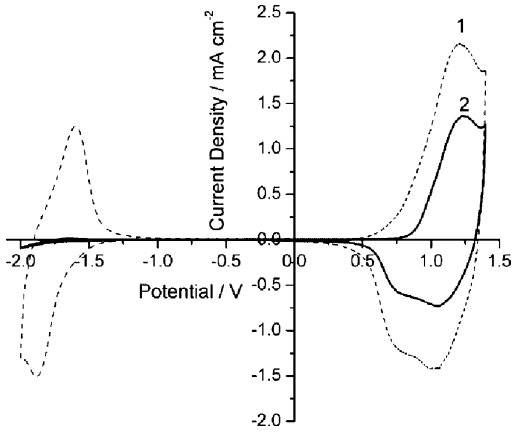

Figure 9. Cyclic voltammograms of (1) ITO/PBT and (2) ITO/PBT/CNx in acetonitrile and 0.1 M $TBAPF_6$.

carbon nitride on its own is not included as it is well established in the literature that these films do not show significant currents in the potential regions examined here.[26] The voltammogram for PBT clearly shows broad anodic and cathodic doping/undoping peaks that are typical of the PBT polymer in nonaqueous conditions.[58] In the anodic region, anodic doping occurs, which corresponds to oxidation of the polymer backbone. In the cathodic region, reduction and n-doping of the polymer backbone takes place, with the electrons being injected from the contact and driving the reduction process.

The voltammetric response for a PBT/CNx film features similar electrochemical behavior to a pristine PBT film in the anodic region. This indicates that electrolyte and solvent are able to penetrate into the PBT through CNx allowing for oxidation to occur, although to a lesser degree than in the case of pristine PBT film. The presence of a pronounced anodic polymer oxidation peak in the voltammogram for the composite material and the absence of current in the potential range where the polymer is not conducting indicate that CNx sputtering did not damage the underlying PBT susbstrate. This was also demonstrated in our previous paper by AFM and conducting AFM measurements.[31] The composite material is oxidized across the entire film and not only at the edges of the electrode as a visual change in color is observed across the whole film during oxidation. Additionally, repeated cycling led to a cracking of the CNx film, which was attributed to the well-known swelling and shrinking of the polymer film in the course of its doping-undoping. These results indicate that the CNx layer adheres well to the PBT layer as it does not delaminate from the surface throughout the entire process, further emphasizing the formation of a stable composite film.

In the cathodic region, however, the behavior of the PBT/CNx composite is strikingly different from that of pristine PBT. Specifically, the composite film showed no ability to be doped in the cathodic region. This is an interesting phenomenon that has been previously observed for donor polymers incorporating an acceptor material,[40,42] and can be related to the fact that electrons injected from the contact are scavenged by the acceptor component and are not able to reduce the polymer phase. This phenomenon is broadly analogous to the well-known fact of fluorescence quenching in donor–acceptor systems (depopulation of the excited states of the donor due to the donor–acceptor electron transfer). These results suggest that CNx behaves as an electron acceptor material with PBT and prevents the n-doping of the polymer film. In the absence of doping, the polymer remains semiconducting and no or very little dark current can flow through the polymer/CNx composite, as compared to the pristine polymer film that becomes fully doped and therefore conducting at negative potentials (Figure 9). Furthermore, the fact that the cathodic doping is not just reduced but is abolished altogether suggests that the acceptor material is located not only at the interface with the donor material but throughout the entire thickness of the composite film. Therefore, we may conclude that CNx indeed can function as an effective electron acceptor material and forms an interpenetrating heterojunction with a conjugated donor polymer such as polybithiophene. Furthermore, CNx vacuum deposition did not damage the polymer film. CNx can also perform well another very important function of the acceptor component and provide efficient conductivity pathways for the captured charge carriers.

4. CONCLUSIONS

The photocurrent generation in composite carbon nitride/conjugated polymer composite films was reported for the first time both in solution and in solid-state devices. It was attributed to the occurrence of the donor–acceptor effect in such composite films with the conjugated polymer acting as a donor and carbon nitride acting as an acceptor. Furthermore, nanoscale structural investigations revealed that such composites may feature a bulk heterojunction structure between PBT and CNx with CNx penetrating the PBT layer and forming finely segregated conducting and semiconducting domains. The results suggest that carbon nitride materials have the potential to become an alternative to fullerenes in organic bulk heterojunction solar cells.

Without the polymer, CNx films did not show any photovoltaic effect, which was related to the abundance of

graphitic domains that short-circuited the semiconducting domains where charge photogeneration could occur. At the same time, CNx films prepared at high nitrogen content and magnetron power did show photoconductivity. Mott−Schottky measurements in electrolyte solution also revealed the formation of a space charge layer consistent with these materials being n-type semiconductors.

The variations in the film properties with the deposition conditions were attributed to the structural reorganization of the film that occurs during the deposition process. It was found that film thickness increased with both the target power and total nitrogen content, whereas the conductivity of the films decreased. The best semiconductor properties were observed for films prepared using increased magnetron power and nitrogen content. The dopant density in such films was also lower. At low deposition powers and nitrogen contents, a significant amount of graphitic carbon was present.

■ ASSOCIATED CONTENT

Supporting Information

Thickness measurements and optical properties of CNx films. This material is available free of charge via the Internet at http://pubs.acs.org.

■ AUTHOR INFORMATION

Corresponding Author

*E-mail: osemenik@uwo.ca (O.A.S.); alain.pailleret@upmc.fr (A.P.). Phone: +1 519 661 2111, ext. 82858 (O.A.S.); + 33 01 44 27 41 69 (A.P.). Fax: +1 519 661 3022 (O.A.S), + 33 01 44 27 40 74 (A.P.).

Author Contributions

The manuscript was written through contributions of all authors. All authors have given approval to the final version of the manuscript.

Notes

The authors declare no competing financial interest.

■ ACKNOWLEDGMENTS

S. Borensztajn is warmly acknowledged for his expertise in FEG-SEM imaging. The financial support of this work by the Natural Sciences and Engineering Research Council of Canada (NSERC), Canada Foundation for Innovation/Ontario Innovation Trust (CFI/OIT), the Academic Development Fund of the University of Western Ontario, and the University of Pierre and Marie Curie (UPMC, Paris, France) is gratefully acknowledged. One of the authors (O.A.S.) is grateful to UPMC for the support of his visit to UPMC as an invited professor. JCB gratefully acknowledges funding from a French Government Award and an ASPIRE student award from the Department of Chemistry, The University of Western Ontario.

■ REFERENCES

(1) Nielsen, T. D.; Cruickshank, C.; Foged, S.; Thorsen, J.; Krebs, F. C. *Sol. Energy Mater. Sol. Cells* **2010**, *94*, 1553−1571.
(2) Helgesen, M.; Sondergaard, R.; Krebs, F. C. *J. Mater. Chem.* **2010**, *20*, 36−60.
(3) Yu, G.; Gao, J.; Hummelen, J.; Wudl, F.; Heeger, A. *Science* **1995**, *270*, 1789−1791.
(4) Guenes, S.; Neugebauer, H.; Sariciftci, N. S. *Chem. Rev.* **2007**, *107*, 1324−1338.
(5) Brabec, C.; Cravino, A.; Meissner, D.; Sariciftci, N.; Fromherz, T.; Rispens, M.; Sanchez, L.; Hummelen, J. *Adv. Funct. Mater.* **2001**, *11*, 374−380.
(6) Sariciftci, N.; Smilowitz, L.; Heeger, A.; Wudl, F. *Science* **1992**, *258*, 1474−1476.
(7) Mihailetchi, V.; van Duren, J.; Blom, P.; Hummelen, J.; Janssen, R.; Kroon, J.; Rispens, M.; Verhees, W.; Wienk, M. *Adv. Funct. Mater.* **2003**, *13*, 43−46.
(8) Blom, P. W. M.; Mihailetchi, V. D.; Koster, L. J. A.; Markov, D. E. *Adv. Mater.* **2007**, *19*, 1551−1566.
(9) Yang, X.; Loos, J. *Macromolecules* **2007**, *40*, 1353−1362.
(10) Krebs, F. C.; Norrman, K. *Prog. Photovolt.* **2007**, *15*, 697−712.
(11) Jorgensen, M.; Norrman, K.; Krebs, F. C. *Sol. Energy Mater. Sol. Cells* **2008**, *92*, 686−714.
(12) Bertho, S.; Janssen, G.; Cleij, T. J.; Conings, B.; Moons, W.; Gadisa, A.; D'Haen, J.; Goovaerts, E.; Lutsen, L.; Manca, J.; Vanderzande, D. *Sol. Energy Mater. Sol. Cells* **2008**, *92*, 753−760.
(13) Brabec, C. J.; Heeney, M.; McCulloch, I.; Nelson, J. *Chem. Soc. Rev.* **2011**, *40*, 1185−1199.
(14) Schwenn, P. E.; Gui, K.; Nardes, A. M.; Krueger, K. B.; Lee, K. H.; Mutkins, K.; Rubinstein-Dunlop, H.; Shaw, P. E.; Kopidakis, N.; Burn, P. L.; Meredith, P. *Adv. Energy Mater.* **2011**, *1*, 73−81.
(15) Sonar, P.; Lim, J. P. F.; Chan, K. L. *Energy Environ. Sci.* **2011**, *4*, 1558−1574.
(16) Li, Z.; Gao, F.; Greenham, N. C.; McNeill, C. R. *Adv. Funct. Mater.* **2011**, *21*, 1419−1431.
(17) Avouris, P.; Chen, Z.; Perebeinos, V. *Nat. Nanotechnol.* **2007**, *2*, 605−615.
(18) Tung, V. C.; Huang, J.; Tevis, I.; Kim, F.; Kim, J.; Chu, C.; Stupp, S. I.; Huang, J. *J. Am. Chem. Soc.* **2011**, *133*, 4940−4947.
(19) Silva, S.; Rafferty, B.; Amaratunga, G.; Schwan, J.; Franceschini, D.; Brown, L. *Diamond Relat. Mater.* **1996**, *5*, 401−404.
(20) Zhou, Z.; Cui, R.; Pang, Q.; Hadi, G.; Ding, Z.; Li, W. *Sol. Energy Mater. Sol. Cells* **2002**, *70*, 487−493.
(21) Alibart, F.; Drouhin, O. D.; Benlahsen, M.; Muhl, S.; Rodil, S. E.; Camps, E.; Escobar-Alarcon, L. *Appl. Surf. Sci.* **2008**, *254*, 5564−5568.
(22) Alibart, F.; Drouhin, O. D.; Lejeune, M.; Benlahsen, A.; Rodil, S. E.; Camps, E. *Diamond Relat. Mater.* **2008**, *17*, 925−930.
(23) Sjostrom, H.; Hultman, L.; Sundgren, J.; Hainsworth, S.; Page, T.; Theunissen, G. *J. Vac. Sci. Technol., A* **1996**, *14*, 56−62.
(24) Yoo, K.; Miller, B.; Kalish, R.; Shi, X. *Electrochem. Solid-State Lett.* **1999**, *2*, 233−235.
(25) Broitman, E.; Hellgren, N.; Wanstrand, O.; Johansson, M.; Berlind, T.; Sjostrom, H.; Sundgren, J.; Larsson, M.; Hultman, L. *Wear* **2001**, *248*, 55−64.
(26) Lagrini, A.; Deslouis, C.; Cachet, H.; Benlahsen, M.; Charvet, S. *Electrochem. Commun.* **2004**, *6*, 245−248.
(27) Monclus, M.; Cameron, D.; Barklie, R.; Collins, M. *Surf. Coat. Technol.* **1999**, *116*, 54−58.
(28) Friedrich, M.; Welzel, T.; Rochotzki, R.; Kupfer, H.; Zahn, D. *Diamond Relat. Mater.* **1997**, *6*, 33−40.
(29) Hultman, L.; Neidhardt, J.; Hellgren, N.; Sjostrom, H.; Sundgren, J. *MRS Bull.* **2003**, *28*, 194−202.
(30) Alibart, F.; Lejeune, M.; Drouhin, O. D.; Zellama, K.; Benlahsen, M. *J. Appl. Phys.* **2010**, *108*, 053504.
(31) Byers, J. C.; Tamiasso-Martinhon, P.; Deslouis, C.; Pailleret, A.; Semenikhin, O. A. *J. Phys. Chem. C* **2010**, *114*, 18474−18480.
(32) Zheng, W.; Sjostrom, H.; Ivanov, I.; Xing, K.; Broitman, E.; Salaneck, W.; Greene, J.; Sundgren, J. *J. Vac. Sci. Technol., A* **1996**, *14*, 2696−2701.
(33) Muhl, S.; Mendez, J. *Diamond Relat. Mater.* **1999**, *8*, 1809−1830.
(34) Hellgren, N.; Johansson, M.; Broitman, E.; Hultman, L.; Sundgren, J. *Phys. Rev. B: Condens. Matter Mater. Phys.* **1999**, *59*, 5162−5169.
(35) Lejeune, M.; Durand-Drouhin, O.; Charvet, S.; Grosman, A.; Ortega, C.; Benlahsen, M. *Thin Solid Films* **2003**, *444*, 1−8.
(36) Alibart, F.; Lejeune, M.; Zellama, K.; Benlahsen, M. *Diamond Relat. Mater.* **2011**, *20*, 409−412.
(37) Alibart, F.; Drouhin, O. D.; Debiemme-Chouvy, C.; Benlahsen, M. *Solid State Commun.* **2008**, *145*, 392−396.

(38) Ferrari, A.; Rodil, S.; Robertson, J. *Phys. Rev. B: Condens. Matter Mater.* **2003**, *67*, 155306.
(39) Semenikhin, O. A.; Hossain, M. M. D.; Workentin, M. S. *J. Phys. Chem. B* **2006**, *110*, 20189−20196.
(40) DiCarmine, P. M.; Wang, X.; Pagenkopf, B. L.; Semenikhin, O. A. *Electrochem. Commun.* **2008**, *10*, 229−232.
(41) Tindale, J. J.; Holm, H.; Workentin, M. S.; Semenikhin, O. A. *J. Electroanal. Chem.* **2008**, *612*, 219−230.
(42) Byers, J. C.; DiCarmine, P. M.; Moustafa, M. M. A. R.; Wang, X.; Pagenkopf, B. L.; Semenikhin, O. A. *J. Phys. Chem. B* **2009**, *113*, 15715−15723.
(43) Arenal, R.; Stephan, O.; Bruno, P.; Gruen, D. M. *Appl. Phys. Lett.* **2009**, *94*, 111905.
(44) Robertson, J.; O'Reilly, E. P. *Phys. Rev. B: Condens. Matter Mater. Phys.* **1987**, *35*, 2946−2957.
(45) Rodil, S.; Muhl, S. *Diamond Relat. Mater.* **2004**, *13*, 1521−1531.
(46) Lazar, G.; Clin, M.; Charvet, S.; Therasse, M.; Godet, C.; Zellama, K. *Diamond Relat. Mater.* **2003**, *12*, 201−207.
(47) Cheah, L.; Shi, X.; Liu, E.; Shi, J. *Appl. Phys. Lett.* **1998**, *73*, 2473−2475.
(48) Katsuno, T.; Nitta, S.; Habuchi, H.; Stolojan, V.; Silva, S. *Appl. Phys. Lett.* **2004**, *85*, 2803−2805.
(49) Peat, R.; Peter, L. *Appl. Phys. Lett.* **1987**, *51*, 328−330.
(50) Peponas, S.; Guedda, M.; Benlahsen, M. *Solid State Commun.* **2008**, *146*, 78−82.
(51) Pleskov, Y. V.; Pimenov, S. M.; Lim, P.; Ralchenko, V. G. *Russ. J. Electrochem.* **2008**, *44*, 861−865.
(52) Robertson, J.; Davis, C. *Diamond Relat. Mater.* **1995**, *4*, 441−444.
(53) Alibart, F.; Peponas, S.; Charvet, S.; Benlahsen, M. *Thin Solid Films* **2011**, *519*, 3430−3436.
(54) Kusano, Y.; Evetts, J.; Somekh, R.; Hutchings, I. *Thin Solid Films* **1998**, *332*, 56−61.
(55) Ilie, A.; Hart, A.; Flewitt, A. J.; Robertson, J.; Milne, W. I. *J. Appl. Phys.* **2000**, *88*, 6002.
(56) Miyajima, Y.; Tison, Y.; Giusca, C. E.; Stolojan, V.; Watanabe, H.; Habuchi, H.; Henley, S. J.; Shannon, J. M.; Silva, S. R. P. *Carbon* **2011**, *49*, 5229.
(57) ElRashiedy, O.; Holdcroft, S. *J. Phys. Chem.* **1996**, *100*, 5481−5484.
(58) Semenikhin, O.; Ovsyannikova, E.; Ehrenburg, M.; Alpatova, N.; Kazarinov, V. *J. Electroanal. Chem.* **2000**, *494*, 1−11.